

Scaling laws for thermal conductivity of crystalline nanoporous silicon based on molecular dynamics simulations

Jin Fang and Laurent Pilon^{a)}

Mechanical and Aerospace Engineering Department, University of California, Los Angeles Henry Samueli School of Engineering and Applied Science, 420 Westwood Plaza, Los Angeles, California 90095, USA

(Received 13 May 2011; accepted 7 August 2011; published online 19 September 2011)

This study establishes that the effective thermal conductivity k_{eff} of crystalline nanoporous silicon is strongly affected not only by the porosity f_v and the system's length L_z but also by the pore interfacial area concentration A_i . The thermal conductivity of crystalline nanoporous silicon was predicted using non-equilibrium molecular dynamics simulations. The Stillinger-Weber potential for silicon was used to simulate the interatomic interactions. Spherical pores organized in a simple cubic lattice were introduced in a crystalline silicon matrix by removing atoms within selected regions of the simulation cell. Effects of the (i) system length ranging from 13 to 130 nm, (ii) pore diameter varying between 1.74 and 5.86 nm, and (iii) porosity ranging from 8% to 38%, on thermal conductivity were investigated. A physics-based model was also developed by combining kinetic theory and the coherent potential approximation. The effective thermal conductivity was proportional to $(1 - 1.5f_v)$ and inversely proportional to the sum $(A_i/4 + 1/L_z)$. This model was in excellent agreement with the thermal conductivity of nanoporous silicon predicted by molecular dynamics simulations for spherical pores (present study) as well as for cylindrical pores and vacancy defects reported in the literature. These results will be useful in designing nanostructured materials with desired thermal conductivity by tuning their morphology. © 2011 American Institute of Physics. [doi:10.1063/1.3638054]

I. INTRODUCTION

Porous silicon has been the subject of intense studies due to its wide range of applications. For example, porous silicon has been used in optoelectronics for its photoluminescence properties.¹ Optoelectronic devices generate heat by Joule heating and by photon absorption. Thus, knowing the thermal conductivity of porous silicon is important for proper thermal management of these devices.² In addition, porous silicon has been used as thermal insulator and sensor in microsystem technology thanks to its low thermal conductivity and rigid solid structure.³ More recently, nanoporous silicon was also found promising in high energetic MEMS devices.^{4–10} The presence of nanosize pores creates very large internal surface area. Combining with oxygen source and heat input, strong exothermic reactions take place within the nanoporous silicon which could be used for microthrusters, microinitiators, and gas generation for actuators.⁹ Here also, the thermal conductivity of nanoporous silicon is essential to the design and operation of these MEMS devices.

Moreover, porous silicon is a potentially efficient thermoelectric material for energy harvesting applications.^{11,12} Thermoelectric materials utilize the Seebeck effect to directly convert a temperature gradient directly into electricity. Their performance is described by the figure of merit ZT given by $ZT = \sigma TS^2/k$, where T is absolute temperature, σ and k are the electrical and thermal conductivities, respectively. The Seebeck coefficient S depends on the temperature and on the material.¹³ Good thermoelectric materials feature high electrical conductivity and high Seebeck coefficient but

low thermal conductivity. However, it is difficult to find such materials due to the interdependence among σ , S , and k .¹³ As a thermoelectric material, bulk dense crystalline Si is considered inefficient with ZT around 0.003 at room temperature.¹² However, according to recent simulations, well-ordered nanoporous silicon with pore diameter between 0.6 and 1.2 nm and porosity between 12% and 30% may feature ZT of about 1.0 at 300 K.¹² This significant increase in ZT was attributed to the large reduction in k accompanied by only moderate changes in σ and S .^{11,12} Practically, a ZT value of about 3.0 could lead to efficient solid state energy conversion.¹³ Thus, the thermal conductivity of nanoporous silicon needs to be tuned in order to further improve its figure of merit. It is therefore, important to first understand and predict thermal transport in nanoporous crystalline silicon.

II. BACKGROUND

A. Molecular dynamics simulations

Molecular dynamics (MD) simulations solve the Newton's equation of motion of individual atoms whose interactions are governed by an empirical interatomic potential. Two main approaches have been developed to predict thermal conductivity using MD simulations, namely (i) the equilibrium Green-Kubo approach and (ii) the direct non-equilibrium molecular dynamics (NEMD) approach.¹⁴ These two approaches have been described in detail in the literature.^{14–19} MD simulations are increasingly used to investigate physical phenomena controlling energy transport in both bulk dense and nanostructured materials. In particular, Lee *et al.*¹¹ investigated the transverse thermal conductivity of nanoporous silicon with periodically arranged

^{a)}Electronic mail: pilon@seas.ucla.edu.

cylindrical pores at 300 K using MD simulations. The authors performed equilibrium MD simulations using the Einstein relation²⁰ similar to the Green-Kubo relation.^{16,17} Note that the simulation cell contained only one cylindrical pore and the atoms at the surface of the pore were passivated with hydrogen atoms. The thermal conductivity predicted by this equilibrium method corresponds to the bulk property. The porosity and pore diameter ranged from 7% to 38% and from 0.63 to 2.26 nm, respectively. The Tersoff type potential was used to model interatomic Si-Si and Si-H interactions.²¹ This potential overestimated the thermal conductivity of dense crystalline Si by about 80% compared with experimental measurements at 300 K.¹¹ The authors indicated that the predicted thermal conductivity of nanoporous Si at 300 K was more than two orders of magnitude smaller than that of dense crystalline silicon.¹¹ They also showed that the thermal conductivity of porous silicon (i) decreased with increasing pore diameter for a given pore spacing, and (ii) increased with increasing pore spacing for a given pore diameter.¹¹

Moreover, the NEMD simulations can predict the thermal conductivity from the temperature gradient and heat flux flowing through a simulation system. It is ideal for investigating finite size effect for structures such as thin films and superlattices.^{14,18} This method had previously been implemented to predict the thermal conductivity of dense solid materials such as silicon,¹⁸ quartz,²² dense and nanoporous amorphous silica.^{23–25} Recently, Lee *et al.*²⁶ investigated the effect of randomly dispersed vacancy defects on the thermal conductivity of crystalline silicon using NEMD simulations with the Tersoff potential. The authors considered tetrahedral, hexahedral, and dodecahedral-like vacancy clusters with vacancy concentration (i.e., porosity) ranging from 0.15% to 1.5%.²⁶ Considering the induced strain fields, their effective diameters were estimated as 1.33, 1.50, and 1.70 nm, respectively. Note that each vacancy cluster contained only 4 to 12 atoms and the maximum vacancy concentration simulated did not exceed 1.5%. The thermal conductivity at 300 K was found to decrease by 95% with porosity of 1.5%. It was not affected by the size of the clusters above the vacancy concentration of 1%.²⁶

B. Physical modeling

The thermal conductivity of nanoporous crystalline materials was reported to depend on both the porosity and the pore size.^{2,11,27–29} Alvarez *et al.*²⁸ studied the influence of porosity and pore size on the thermal conductivity of crystalline porous silicon using the phonon hydrodynamics approach. The authors considered monodisperse spherical pores randomly dispersed in a three-dimensional crystalline silicon matrix. They expressed the effective thermal conductivity as,²⁸

$$k_{eff} = k_m \frac{1}{\frac{1}{f(f_v)} + 18f_v \frac{(l/d_p)^2}{1 + 2A'(l/d_p)} \left(1 + \frac{3}{\sqrt{2}}\sqrt{f_v}\right)}, \quad (1)$$

where k_m is the thermal conductivity of dense matrix material, f_v is the porosity, d_p is the pore diameter, l is the

dominant phonon mean free path (MFP) in bulk dense silicon, $f(f_v) = (1 - f_v)^3$ based on percolation theory,^{30,31} and A' is a function of l/d_p expressed by Millikan³² as $A' = 0.864 + 0.29 \exp(-0.625d_p/l)$. The authors compared predictions of Eq. (1) with experimental results at room temperature for electrochemically etched porous silicon with porosity ranging from 40% to 90% and vertical cylindrical pores with radius ranging from 1 to 100 nm.²⁸ Good agreement was found by taking the dominant phonon MFP l for silicon at 300 K as 40 nm.²⁸ However, this value was smaller than that of about 300 nm suggested in the literature.^{33,34} This latter value was derived by considering the phonon dispersion and assuming that only the acoustic phonons contributed to heat transfer.^{33,34}

As previously discussed, Lee *et al.*¹¹ investigated the transverse thermal conductivity of nanoporous silicon with cylindrical pores at room temperature using MD simulations. The authors also correlated their results with the ballistic-diffusive model developed by Prasher²⁷ for two-dimensional systems and expressed as,²⁷

$$k_{eff} = k_m \frac{1}{\frac{1}{f(f_v)} + \alpha \frac{\sqrt{f_v}}{F(f_v)d_p}}, \quad (2)$$

where $F(f_v) = \sqrt{4f_v/\pi}(\sin^{-1} \sqrt{4f_v/\pi} - \pi/2) + \sqrt{1 - 4f_v/\pi}$ and $f(f_v) = (1 - f_v)(1 + \beta f_v^\gamma)$. The three empirical fitting parameters α , β , and γ were fitted against MD simulation results for k_{eff} as $\alpha = 50.9$, $\beta = 1821.1$, and $\gamma = 1.9$, respectively.¹¹

The present study aims to predict the thermal conductivity of crystalline nanoporous silicon using NEMD simulations. Multiple spherical pores organized in a simple cubic lattice were introduced into a crystalline silicon matrix. First, the simulation procedure was validated with results for dense crystalline silicon reported in the literature.^{18,35,36} Then, the thermal conductivity of nanoporous crystalline silicon was computed at 500 K for various system morphology including porosity, pore diameter, and system length. Finally, a physics-based model predicting the effects of these parameters on the thermal conductivity of nanoporous silicon was developed.

III. ANALYSIS

A. Thermal conductivity prediction using NEMD simulations

The detailed procedure of the NEMD simulations used in the present study has already been described by Coquil *et al.*²⁵ and need not be repeated. In brief, the thermal conductivity was estimated using the so-called Muller-Plathe method.^{19,23} It consists of imposing a heat flux q_z'' along the z -direction and determining the resulting temperature gradient dT_{MD}/dz to estimate the thermal conductivity as,¹⁸

$$k = -\frac{q_z''}{dT_{MD}/dz}. \quad (3)$$

The heat flux was imposed by a velocity swapping technique described in the literature.^{19,23} To do so, the atoms with the

largest kinetic energy (i.e., the hottest) in the heat sink were exchanged with those with the lowest kinetic energy (i.e., the coolest) in the heat source. The simulation cell was first divided into an even number of slices. The temperature of each slice and its gradient were calculated by averaging the atomic kinetic energy over time as well as overall the atoms in the slice. The temperature $T_{MD}(z)$ of a slice along the z -direction (i.e., the direction of the heat flux) at every time step was determined from the classical statistical mechanics equipartition theorem as,²³

$$T_{MD}(z) = \frac{1}{3n_k k_B} \sum_{i=1}^{n_k} m_i v_i^2, \quad (4)$$

where $k_B = 1.38 \times 10^{-23} \text{ m}^2 \text{ kg/s}^2 \text{ K}$ is the Boltzmann's constant, n_k is the number of atoms in the slice about z , and m_i and v_i are the mass and velocity of individual atoms i , respectively. The temperature of each slice was then averaged over multiple time steps. The number of atoms per slice n_k was chosen to be larger than 32 following Schelling *et al.*¹⁸ After reaching steady state, a temperature profile $T_{MD}(z)$ decreasing from the center to the ends of the simulation cell could be estimated using Eq. (4). A total number of 6 to 8×10^6 steps were simulated for a microcanonical or NVE ensemble, in which the total number of atoms, total volume, and total energy of the system were conserved. In addition, periodic boundary conditions were imposed in all directions. Finally, the thermal conductivity was retrieved using Eq. (3) by averaging over the last 2×10^6 time steps. The numerical procedure was implemented using the large-scale atomic/molecular massively parallel simulator (LAMMPS).³⁷ Simulations were run in parallel on 32 to 128 64-bit nodes with 1024 to 2048 MB of RAM.

It should be noted that the expression for temperature $T_{MD}(z)$ given by Eq. (4) is widely used in MD simulations. However, T_{MD} represents the real temperature T only if the latter is much larger than the Debye temperature T_{Debye} .³⁸ In cases when the system temperature is lower than T_{Debye} , T_{MD} needs to be corrected for quantum effects.³⁸ For silicon, $T_{Debye} = 650 \text{ K}$ (Ref. 18) and according to Volz and Chen³⁸ and Tang,³⁹ quantum corrections are negligible when T_{MD} exceeds 500 K for crystalline silicon systems.

B. Validation

MD simulations were first validated with dense crystalline silicon. The well established two and three-body interactions Stillinger and Weber (SW) potential⁴⁰ was used. It is known to successfully describe the elastic constants and thermal expansion coefficients, as well as phonon dispersion relations of dense silicon.⁴¹⁻⁴³ It was also previously used to model silicon thermal conductivity above 500 K.¹⁸ Here, simulation systems consisted of six silicon unit cells in both the x - and y -directions, with each unit cell consisting of a diamond cubic arrangement of eight silicon atoms. The lattice constant a of each unit cell was 5.43 Å. On the other hand, the number of unit cells along the z -direction varied from 48 to 384. Results for thermal conductivity were analyzed as a function of the simulation system length L_z ranging from

26 to 104 nm. The total number of atoms varied from 13 824 to 55 294. Simulations were performed at both 500 and 1000 K. The simulation time step was set to be 0.55 fs and simulations were run for a total of 6×10^6 time steps. This corresponded to an effective time of 3.3 ns which was more than twice as long as the total time used by Schelling *et al.*¹⁸ and well above the 1 ns limit necessary to reach a steady-state temperature profile.¹⁸ The equations of motion were integrated using a velocity Verlet algorithm.¹⁵ The rate of velocity exchanges was chosen so that the corresponding heat flux was approximately $1.8 \times 10^{11} \text{ eV/nm}^2\cdot\text{s}$, in agreement with that used by Schelling *et al.*¹⁸ The simulation systems were divided into slices corresponding to 1/4 of a silicon unit cell. Note that the temperature profile was found to have already converged after the first 2×10^6 steps.

The temperature profile was linear except for the slices within the heat source and heat sink regions, both corresponding to about 20% of the simulation system length. The nonlinearity in temperature observed around those regions was attributed to the strong scattering caused by the heat source and sink.⁴⁴ The linear part of the temperature profile was fitted with a linear function, $T_{MD}(z)$, and the resulting gradient, dT_{MD}/dz , was used in Eq. (3) to estimate the thermal conductivity. The gradients estimated for the two different linear regions, on each side of the heat source, typically differed by less than 10%. This difference was used to estimate the error associated with the retrieved thermal conductivity. Note that the system length L_z represents half of the total length of the simulation cell along the z -direction.

Figure 1 plots $1/k$ as a function of $1/L_z$ at 500 and 1000 K along with results previously reported by Schelling *et al.*¹⁸ and bulk properties for natural and isotopically enriched silicon reported in the literature.^{35,36} It establishes that results obtained in the present study were in excellent agreement with those previously reported by Schelling *et al.*¹⁸ In

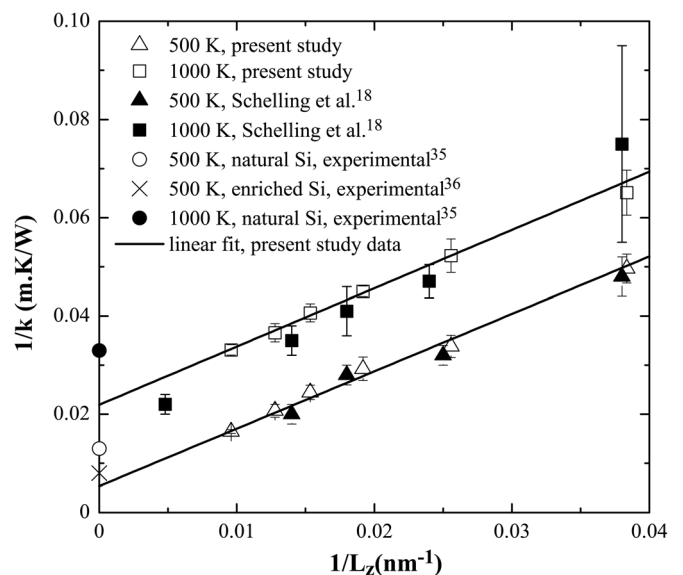


FIG. 1. Predicted values of $1/k$ as a function of $1/L_z$ for crystalline silicon at 500 and 1000 K along with similar results reported by Schelling *et al.* (Ref. 18) Experimental data for bulk natural silicon (Ref. 35) and isotopically enriched pure silicon (Ref. 36) are also displayed.

addition, the bulk thermal conductivity can be estimated by extrapolating the linear fit (solid lines) for $1/k$ versus $1/L_z$ as $1/L_z$ tends to zero or L_z tends to infinity.¹⁸ Then, the thermal conductivity of bulk silicon was found to be 141 ± 25 W/m·K at 500 K and 46 ± 2 W/m·K at 1000 K. The measured thermal conductivity of natural Si at 500 and 1000 K were about 80 and 30 W/m·K, respectively.³⁵ That of isotopically enriched Si, known to contain fewer defects than natural Si, was estimated to be 120 W/m·K at 500 K.^{18,36} This was in reasonable agreement with the present MD simulations results.

C. Thermal conductivity of nanoporous silicon

In order to simulate crystalline nanoporous silicon, simulation cells of crystalline silicon were first generated. Here, the simulation cells had the same size (6 to 12 unit cells) along both the x - and y -directions and had 48 to 480 unit cells along the z -direction. Then, spherical pores, in a simple cubic arrangement, were introduced by removing silicon atoms within a spherical region along the centerline of the crystalline lattice. Figure 2 shows the 2D atomic structures of a typical crystalline nanoporous silicon phase with two pores, 2.6 nm in diameter, inserted in a $3.26 \times 3.26 \times 6.52$ nm³ simulation cell. The structure represented a cross-section in the y - z plane which intercepted the center of pores. Note that, in the present study, there was no passivation on the pore surface, i.e., silicon atoms on the pore surface have dangling bonds.

Here also, the time step was 0.55 fs. Initially, the system temperature was uniform and set to be 515 ± 15 K by imposing constant number of atoms, volume and temperature (NVT ensemble) for 20 000 time steps. Then, the system was set to equilibrium under constant number of atoms, volume and energy (NVE ensemble) condition for another 20 000 time steps. Finally, the simulation was performed in the NVE ensemble for 6 to 8×10^6 time steps with velocity exchange rate adjusted to impose a heat flux of approximately 1.8×10^{11} eV/nm²·s (i.e., 2.9×10^{10} W/m²). Note that the pore shape remained spherical throughout the simulations. The z -direction of the simulation cell was divided into slices corresponding to 1/2 of a silicon unit cell and

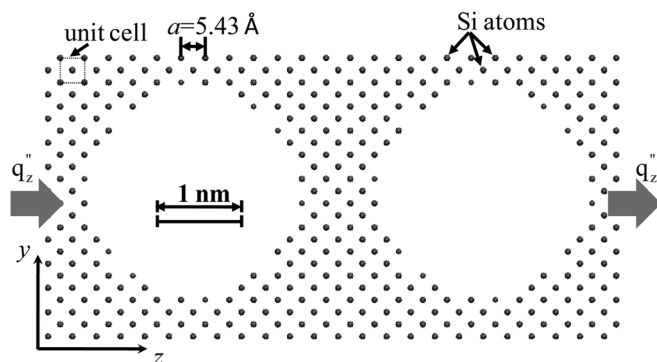


FIG. 2. Typical atomic structures of the nanoporous crystalline silicon phase with two spherical pores of 2.6 nm in diameter aligned along the z -direction of a $3.26 \times 3.26 \times 6.52$ nm³ simulation cell. This 2D representation corresponds to the projection of 1 nm thick slab in the out-of-plane direction.

containing more than 50 atoms. The procedure used to estimate the temperature gradient and to calculate the thermal conductivity was identical to that previously described for dense silicon. The temperature profile was found to have already converged after the first 4×10^6 steps.

Finally, Table I summarizes the values of porosity f_v , spherical pore diameter d_p , cross-sectional area A_c , system length L_z , and pore number N of the crystalline nanoporous silicon systems investigated in the present study. The porosity ranged from 8% to 38% while pore diameter varied from 1.74 to 5.86 nm. The system length was between 13 and 130 nm corresponding to 4 to 32 aligned pores.

IV. RESULTS AND DISCUSSION

A. Effects of system length and pore diameter

Figures 3(a) and 3(b) show the predicted effective thermal conductivity at 500 K of crystalline nanoporous silicon k_{eff} as a function of system length L_z for different pore diameters d_p with porosity f_v equal to 27% and 38%, respectively. They indicate that the thermal conductivity of nanoporous crystalline silicon was more than one order of magnitude smaller than that of dense crystalline silicon at 500 K (see Fig. 1).^{18,35,36} This was due to the fact that the presence of the nanosize pores greatly enhances phonon scattering. Note that similar reduction in thermal conductivity was observed for only 1.5% vacancy concentration as reported by Lee *et al.*²⁶ This could be attributed to the facts that vacancy defects introduced large strain fields in regions of the materials with size comparable to the pore diameter used in the present study.²⁶ These randomly distributed defect-induced strain fields caused large rate of phonon scattering by clusters and effectively obstruct the cross-sectional area for phonon transport.²⁶ In addition, Fig. 3 also establishes that the thermal conductivity of crystalline nanoporous silicon systems for a given porosity (i) increased with increasing L_z for a given pore diameter d_p and (ii) increased with increasing pore diameter d_p for a given length L_z . Similar results and conclusions were found for the other values of porosity investigated (Table I).

TABLE I. Summary of simulated crystalline nanoporous silicon systems with various porosity, pore diameter, cross-section area, system length, and pore number.

Porosity %	Pore diameter d_p (nm)	Cross-section area A_c (nm ²)	Length L_z (nm)	Pore number N
8	1.74	3.26×3.26	13 to 104	4 to 32
8	2.93	5.43×5.43	22 to 109	4 to 20
15	2.17	3.26×3.26	13 to 104	4 to 32
15	2.88	4.34×4.34	17 to 104	4 to 24
27	2.61	3.26×3.26	13 to 104	4 to 32
27	3.48	4.34×4.34	17 to 104	4 to 24
27	4.34	5.43×5.43	22 to 109	4 to 20
27	5.21	6.52×6.52	26 to 130	4 to 20
38	2.93	3.26×3.26	13 to 104	4 to 32
38	3.91	4.34×4.34	17 to 104	4 to 24
38	4.89	5.43×5.43	22 to 130	4 to 24
38	5.86	6.52×6.52	26 to 130	4 to 20

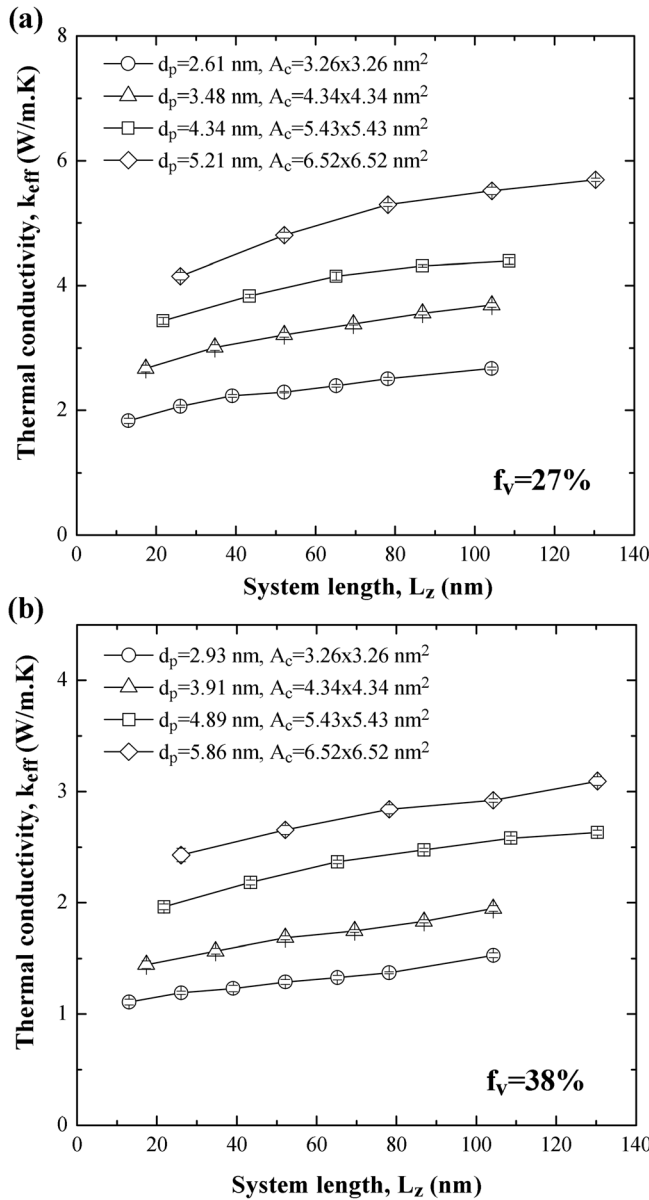


FIG. 3. Predicted effective thermal conductivity of crystalline nanoporous silicon at 500 K as a function of system length L_z for porosity (a) $f_v = 27\%$ and (b) $f_v = 38\%$ along with various pore diameters d_p and simulation cell cross-section A_c .

Moreover, it is interesting to note that Coquil *et al.*²⁵ established that the system length had no effect on the thermal conductivity of amorphous nanoporous SiO₂ when the system length was larger than approximately 5 nm for $d_p = 1.8$ nm and $f_v = 25 \pm 2\%$.²⁵ The different behavior observed with crystalline nanoporous Si can be attributed to their crystalline nature in which phonon modes have significantly longer MFP than in amorphous materials.

B. Effect of porosity

Figure 4 shows the thermal conductivity of nanoporous silicon at 500 K as a function of system length for porosity ranging from 8% to 38%. Here, the pore diameter d_p was maintained at 2.8 ± 0.2 nm and the porosity of nanoporous

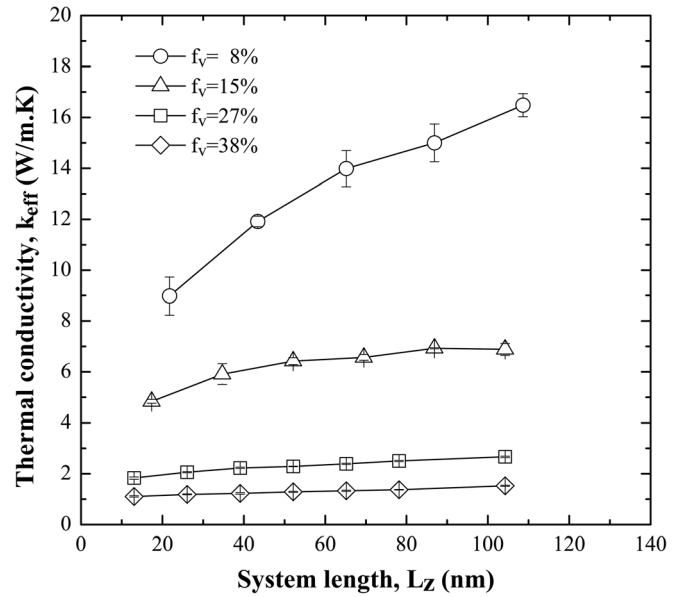


FIG. 4. Predicted effective thermal conductivity of crystalline nanoporous silicon at 500 K as a function of system length for pore diameter $d_p = 2.8 \pm 0.2$ nm and porosity f_v between 8% and 38%.

silicon systems was adjusted by varying the cross-sectional area A_c . It is evident that the thermal conductivity decreased with increasing porosity. In addition, the system length L_z had stronger effect on thermal conductivity for systems with smaller porosity. For example, the thermal conductivity of nanoporous silicon with porosity $f_v = 8\%$ and 38% increased by 85% and 40%, respectively, as L_z increased from 22 to 109 nm. This was due to the fact that, in systems with large porosity, phonon scattering by pores dominated over phonon scattering by film boundaries.

C. Bulk thermal conductivity of nanoporous silicon

The bulk thermal conductivity of nanoporous Si can be determined by linear extrapolation of $1/k$ versus $1/L_z$ as $L_z \rightarrow \infty$.¹⁸ Sellan *et al.*⁴⁵ indicated that the minimum system length used should be comparable to the largest MFP of the dominant phonons. The authors further defined the maximum thermal conductivity k_{max} that can be accurately predicted using the linear extrapolation procedure with a minimum system length L_{min} as,⁴⁵

$$k_{\text{max}} = \frac{L_{\text{min}} k_B v_g}{6a^3}, \quad (5)$$

where a is the lattice constant and v_g is the average phonon group velocity given by,⁴⁵

$$v_g = \frac{1}{3}(v_{g,L} + 2v_{g,T}), \quad (6)$$

where $v_{g,L}$ and $v_{g,T}$ are the longitudinal and transverse phonon group velocities, respectively. Note that the above requirement was validated against results of MD simulations for argon and dense crystalline silicon.^{18,45} Here, we further expressed the group velocities $v_{g,L}$ and $v_{g,T}$ in nanoporous crystalline Si as,⁴⁶

$$v_{g,L} = [(K_{eff} + 4G_{eff}/3)/\rho_{eff}]^{1/2} \quad \text{and} \quad (7a)$$

$$v_{g,T} = (G_{eff}/\rho_{eff})^{1/2}, \quad (7b)$$

where K_{eff} , G_{eff} , and ρ_{eff} are the effective bulk modulus, shear modulus, and density of the nanoporous material, respectively.⁴⁶ For porous material of porosity f_v , the effective bulk modulus K_{eff} has been expressed as,⁴⁷

$$K_{eff} = K_m \left[1 - f_v \left(1 + \frac{3K_m}{4G_m} \right) \right], \quad (8)$$

where K_m and G_m are the bulk and shear modulus of the continuous dense matrix. Similarly, the effective shear modulus G_{eff} can be expressed as,⁴⁷

$$G_{eff} = G_m \left[1 - f_v \left(1 + \frac{6\lambda_m + 16G_m}{9\lambda_m + 14G_m} \right) \right], \quad (9)$$

where λ_m is the Lamé's elastic constant of the dense matrix.⁴⁷ In addition, the effective density ρ_{eff} is given by $\rho_{eff} = \rho_m(1 - f_v)$. The density ρ_m , the bulk modulus K_m , the shear modulus G_m , and the Lamé's constant λ_m for the dense crystalline silicon matrix were calculated from previously reported MD simulations using the Stillinger-Weber potential as 2300 kg/m³, 71.5 GPa, 52.4 GPa, and 36.6 GPa, respectively.⁴² For comparison, the experimental data for ρ_m , K_m , G_m , and λ_m were 2329 kg/m³, 59.6 GPa, 79.6 GPa, and 6.5 GPa, respectively.⁴⁸ Then, the phonon group velocities $v_{g,L}$, $v_{g,T}$, and v_g of nanoporous silicon were calculated using Eqs. (6) to (9). Finally, considering that the minimum system length L_{min} simulated was 50 nm, i.e., $1/L_z < 0.02 \text{ nm}^{-1}$, the maximum thermal conductivity k_{max} predicted by Eq. (5) ranged between 3 and 5 W/m-K for systems with porosity between 8% and 38%. Note that the same conclusions were reached by using the above experimentally measured elastic properties.⁴⁸

Figures 5(a) and 5(b) show the predicted values of $1/k_{eff}$ at 500 K as a function of $1/L_z$ for crystalline nanoporous silicon with porosities of 27% and 38%, respectively. Systems satisfying $1/L_z < 0.02 \text{ nm}^{-1}$ were used for linear extrapolation. Except for systems with 8% porosity, the predicted thermal conductivity of bulk nanoporous silicon k_{eff} ($L_z \rightarrow \infty$) was less than or equal to k_{max} , confirming the validity of the linear extrapolation of $1/k_{eff}$ versus $1/L_z$.⁴⁵ For systems with 8% porosity, simulations of systems significantly longer than those simulated would be required.

D. Physical modeling

1. Effective medium approximations

The effect of porosity on various properties of porous materials is usually accounted for by some effective medium approximations (EMAs). Numerous EMAs have been developed in order to predict the effective thermal conductivity k_{eff} of porous materials.^{25,49} Here, the pores in nanoporous silicon are so small that their thermal conductivity can safely be neglected as explained in Refs. 25 and 50. Then, EMAs typically provide expressions for k_{eff} as the product of the

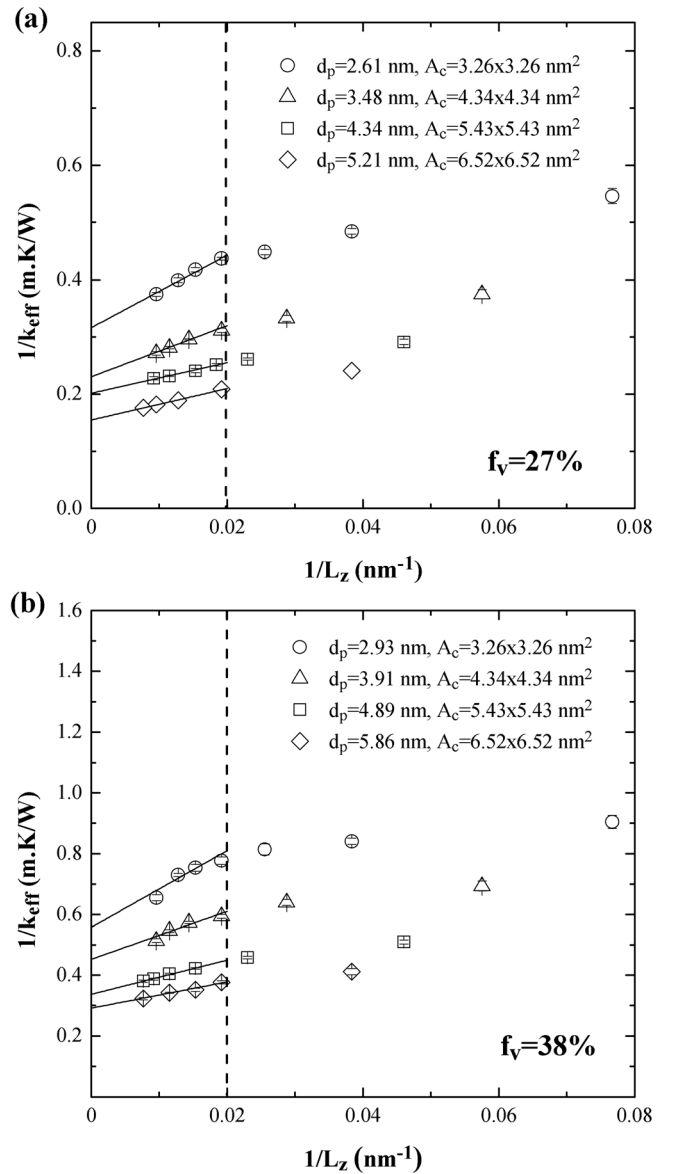


FIG. 5. Predicted values of $1/k_{eff}$ of crystalline nanoporous silicon at 500 K as a function of $1/L_z$ for porosity (a) $f_v = 27\%$ and (b) $f_v = 38\%$ along with various pore diameter d_p and simulation cell cross-section A_c . Linear extrapolation used data satisfying $1/L_z < 0.02 \text{ nm}^{-1}$ ($L_z > 50 \text{ nm}$).

matrix thermal conductivity k_m and a function of porosity $\Psi(f_v)$, i.e., $k_{eff} = k_m \Psi(f_v)$. For example, the Russell model⁵¹ gives $\Psi_{Russell}(f_v) = (1 - f_v^{2/3}) / (1 - f_v^{2/3} + f_v)$ while the Eucken model⁵² uses $\Psi_{Eucken}(f_v) = (1 - f_v) / (1 + f_v/2)$. These models were previously used to model the effective thermal conductivity of microporous silicon with periodically aligned cylindrical pores and porosity of 23% and 26%.^{53,54} Note that these two functions behave similarly and the maximum relative difference between them is about 6% for porous Si of any porosity. In addition, the coherent potential model is expressed as,^{55,56}

$$k_{eff} = k_m \Psi_{cp}(f_v) = k_m (1 - 1.5f_v). \quad (10)$$

This model was first derived by Landauer⁵⁵ for the effective dielectric properties of random mixtures of spherical inclusions in a continuous matrix. The main assumption was that

“a region of type 1 is not preferentially surrounded by either other regions of type 1 or by regions of type 2.”⁵⁵ Therefore, porous materials having very small or very large porosity do not satisfy this assumption. Cahill and Allen⁵⁶ successfully applied the coherent potential model to predict the thermal conductivity of Vycor glass from 30 to 300 K with pore diameter and porosity approximately equal to 10 nm and 30%, respectively. More recently, this model was also found to agree well with predictions of thermal conductivity of amorphous mesoporous silica at 300 K obtained by non-equilibrium MD simulations.²⁵

Finally, note that the above EMAs do not directly account for the effect of pore diameter. However, Figs. 3 and 5 show that d_p has significant effect on k_{eff} for a given porosity. Thus, the coherent potential model and most other EMAs, in their conventional form $k_{eff} = k_m \Psi(f_v)$, are inadequate to predict the effective thermal conductivity of crystalline nanoporous media.

2. Effect of interfacial area concentration

It has been established that the reduction of thermal conductivity of nanocomposite material is mainly due to phonon scattering by interfaces.^{11,57-59} The phonon-interface scattering rate is known to increase with increasing interfacial area concentration A_i (m^{-1}) defined as the surface area of interface per unit volume of nanocomposite material.⁵⁷⁻⁵⁹ In porous material with spherical pores arranged in a simple cubic lattice, the interfacial area concentration can be expressed as $A_i = 6f_v/d_p$. Thus, for a given porosity f_v , A_i increases with decreasing pore diameter d_p . Figure 3 suggests that k_{eff} decreased not only with increasing f_v but also with decreasing d_p and thus with increasing A_i .

Moreover, the systems simulated in the present study fell in the ballistic regime characterized by $l/d_p \gg 10$.⁶⁰ Then, the phonon hydrodynamics model given by Eq. (1) for spherical pores simplifies to,

$$k_{eff} = k_m \frac{1}{1.3l \left(1 + \frac{3}{\sqrt{2}} \sqrt{f_v}\right) A_i}. \quad (11)$$

The relative difference between predictions by Eqs. (1) and (11) for nanoporous silicon systems investigated in the present study was less than 1%. More importantly, Eq. (11) suggests that the thermal conductivity of nanoporous silicon is inversely proportional to A_i .

Similarly, for cylindrical pores with the same ranges of pore diameter and porosity explored in this study, the ballistic diffusive model given by Eq. (2) simplifies to $k_{eff} = k_m \alpha \sqrt{f_v} F(f_v)/A_i$, where for periodically arranged cylindrical pores $A_i = 4f_v/d_p$. Here also, the thermal conductivity appears to be inversely proportional to A_i .

Unfortunately, predictions by Eq. (11) underestimated the thermal conductivity computed by our MD simulations by about 90% at 500 K using $k_m = 80$ W/m·K for high purity crystalline silicon³⁵ and $l \simeq 140$ nm.³³ To improve the predictions of Eq. (11), the MFP l could be treated as a fitting parameter. Alternatively, a new physics-based model was developed in the present study.

3. Modeling

This section presents a model for the effective thermal conductivity of mesoporous Si based on kinetic theory and able to simultaneously account for the effects of porosity, interfacial area concentration, and system length. The kinetic theory expresses the thermal conductivity k_m of the dense matrix in nanoporous materials as,⁶¹

$$k_m = \frac{1}{3} C_{v,m} v_{g,m}^2 \tau_{tot}. \quad (12)$$

The total relaxation time τ_{tot} includes the contributions from (i) phonon Umklapp scattering τ_U as well as phonon scattering by (ii) pores τ_{ph-p} , and (iii) film boundaries τ_{ph-b} . Here, Umklapp scattering rate was estimated based on the phonon MFP in bulk dense silicon as $\tau_U^{-1} = v_{g,m}/l$ where $l \simeq 140$ nm.³³ The relaxation time for phonon scattering by large defect aggregates⁶² was adopted to account for phonon-pore scattering. It was expressed as $\tau_{ph-p}^{-1} = v_{g,m} n \pi d_p^2/4$, where n is the number density of pores of diameter d_p . For spherical pores, $n = 6f_v/(\pi d_p^3)$ so that the phonon-pore scattering rate can be expressed as $\tau_{ph-p}^{-1} = v_{g,m} A_i/4$. This corresponds to an average phonon-pore scattering MFP of $4/A_i$ in good agreement with that derived by Minnich and Chen⁵⁷ for phonon-interface scattering in nanocomposites. In addition, phonon-boundary scattering can be expressed as $\tau_{ph-b}^{-1} = v_{g,m} L_z/4$,³⁵ where L_z corresponds to the thickness of nanoporous silicon thin films. In nanoporous materials, Umklapp scattering is typically negligible compared with phonon scattering by pores and by film boundaries, i.e., $\tau_U^{-1} \ll \tau_{ph-p}^{-1}$ and $\tau_U^{-1} \ll \tau_{ph-b}^{-1}$. These conditions can also be formulated in terms of pore number density or porosity as $n \gg 4/(l\pi d_p^2)$ or $f_v \gg 2d_p/(3l)$ and in terms of system length as $L_z \ll l$, respectively. In the present study, the number density of pores n

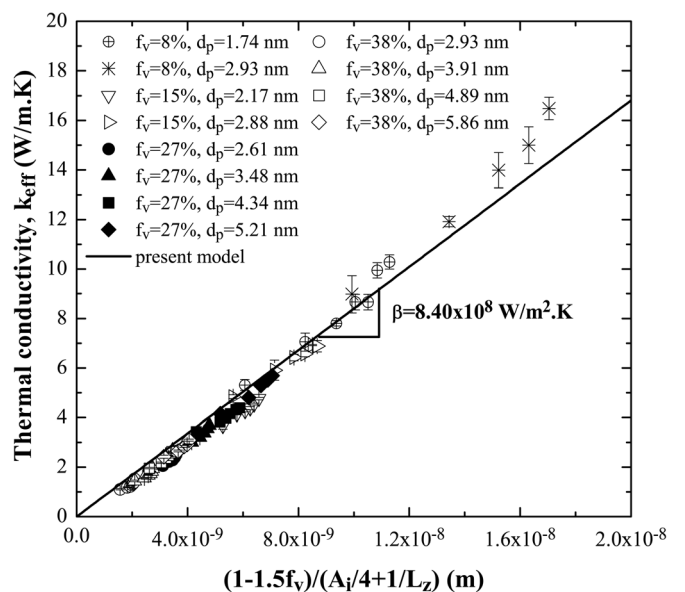


FIG. 6. Effective thermal conductivity k_{eff} as a function of $(1 - 1.5 f_v)/(A_i/4 + 1/L_z)$ of all crystalline nanoporous silicon systems simulated at 500 K for porosity f_v ranging between 8% and 38%, pore diameter d_p between 1.74 and 5.86 nm, and system length between 13 and 130 nm. Predictions by Eq. (15) are also shown with $\beta = 8.40 \times 10^8$ W/m²·K.

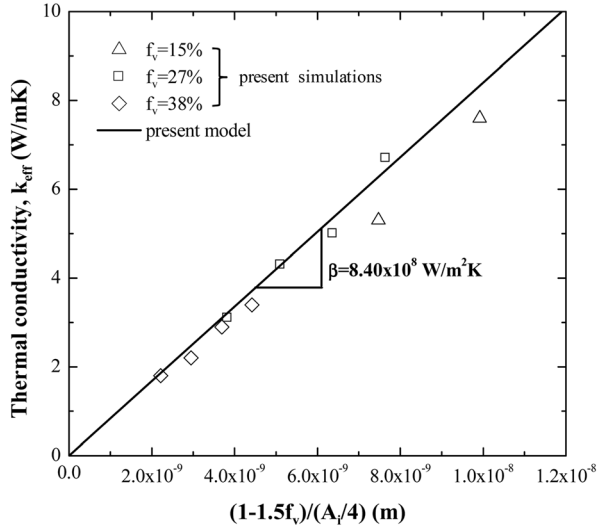
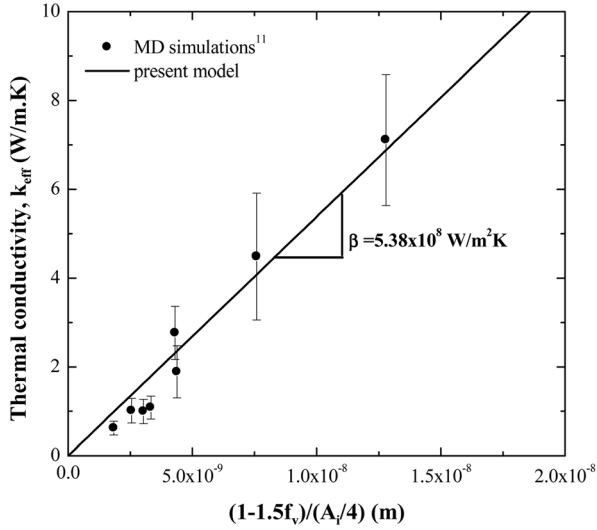
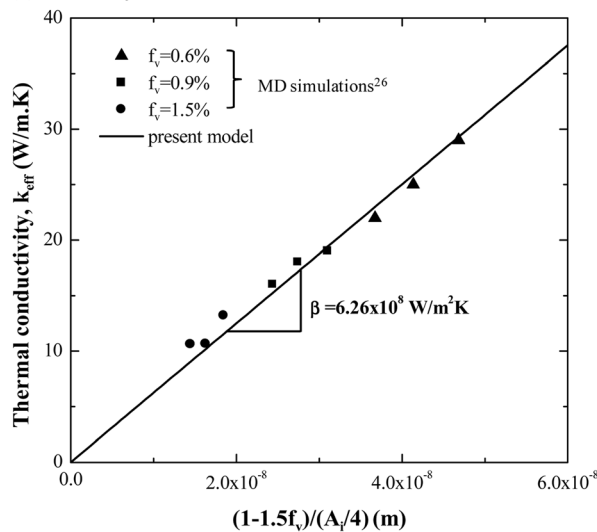
(a) spherical pores**(b) cylindrical pores****(c) vacancy defects**

FIG. 7. Effective bulk thermal conductivity k_{eff} as a function of $(1 - 1.5f_v)/(A_i/4)$ for nanoporous silicon with (a) spherical pores (present study) at 500 K, (b) periodically arranged cylindrical pores at 300 K (Ref. 11), and (c) vacancy defects (Ref. 26) for various values of porosity and pore diameter. Predictions by Eq. (15) are also shown with (a) $\beta = 8.40 \times 10^8$ W/m²·K, (b) $\beta = 5.38 \times 10^8$ W/m²·K, and (c) $\beta = 6.26 \times 10^8$ W/m²·K.

was at least 10 times larger than $4/(\pi d_p^2)$ for all systems simulated. This verified that Umklapp scattering was negligible compared with phonon scattering by pores. Then, according to Matthiessen's rule, the total relaxation time τ_{tot} can be expressed as,³⁵

$$\frac{1}{\tau_{tot}} = \frac{1}{\tau_{ph-p}} + \frac{1}{\tau_{ph-b}} = v_{g,m} \left(\frac{A_i}{4} + \frac{1}{L_z} \right). \quad (13)$$

Combining EMAs, accounting for the effect of porosity on k_{eff} , with the matrix thermal conductivity k_m , accounting for the effect of phonon-pore scattering, the effective thermal conductivity of nanoporous silicon systems can be expressed as,

$$k_{eff} = k_m \Psi(f_v) = \frac{1}{3} C_{v,m} v_{g,m} \frac{\Psi(f_v)}{A_i/4 + 1/L_z}. \quad (14)$$

It is evident that as L_z tends to infinity, the bulk effective thermal conductivity k_{eff} is inversely proportional to A_i in agreement with the phonon hydrodynamic model for spherical pores²⁸ and the ballistic diffusive model for cylindrical pores in the ballistic regime.²⁷

Furthermore, the specific heat $C_{v,m}$ and the group velocity $v_{g,m}$ of the silicon matrix may differ from those of dense bulk silicon due to band folding and phonon confinement effect.^{63,64} In fact, Hopkins *et al.*⁶⁴ recently observed, using the plane-wave expansion technique,⁶⁵ a large reduction in phonon group velocity in single crystalline nanoporous silicon films made by phononic crystal patterning. The main purpose of the present study was to investigate the scaling laws predicting the effects of morphological parameters on the thermal conductivity of nanoporous silicon. To facilitate the scaling analysis and considering the approximate nature of potentials used in MD simulations, the product $C_{v,m} v_{g,m}/3$ was substituted by a semiempirical parameter β so that the effective thermal conductivity can be written as,

$$k_{eff} = \beta \frac{\Psi(f_v)}{A_i/4 + 1/L_z}, \quad (15)$$

where β depends only on temperature, on the matrix materials, and possibly on the choice of interatomic potential. Note that equilibrium MD simulations with the Green-Kubo theorem could be used to predict phonon dispersion and density of state as well as specific heat and group velocity in silicon nanostructures.⁶³ However, this falls outside the scope of the present study.

Figure 6 plots k_{eff} from the MD simulations as a function of $(1 - 1.5f_v)/(A_i/4 + 1/L_z)$ for all values of porosity, pore diameter, and system length investigated in the present study (Table I). It is remarkable that nearly all data points previously scattered (see Figs. 3 and 4) collapsed onto a single straight line. This indicates that the present model successfully captured the effects of various system morphology simultaneously. Here also, the systems with porosity $f_v = 8\%$ showed relatively large deviations from the other systems. This could be attributed to the fact that the small porosity systems do not satisfy the assumption of the coherent potential model,⁵⁵ as previously discussed. In addition, Fig. 6

shows that the effective thermal conductivity k_{eff} for all systems can be linearly related to the present model by using a slope of $\beta = 8.40 \times 10^8 \text{ W/m}^2\cdot\text{K}$ with a coefficient of determination $R^2 = 0.99$. Note that using the Russell model $\Psi_{Russell}(f_v)$ resulted in $\beta = 7.72 \times 10^8 \text{ W/m}^2\cdot\text{K}$ with $R^2 = 0.97$.

Figure 7 plots the effective bulk thermal conductivity k_{eff} as a function of $(1 - 1.5f_v)/(A_i/4)$ for nanoporous silicon with (a) spherical pores computed in the present study as well as, (b) periodically arranged cylindrical pores,¹¹ and (c) vacancy defects²⁶ for various values of porosity and pore diameter reported in other MD simulations. Note that the latter used the Tersoff potential instead of the Stillinger-Weber potential. This suggests that the linear relationship between k_{eff} and $(1 - 1.5f_v)/(A_i/4)$ is independent of the choice of potential although the coefficient of proportionality β may not. Also, note that in Lee *et al.*'s study,²⁶ the 0.15% vacancy concentration did not satisfy the ballistic transport assumption and was not included in the plot. Here also, the effective bulk thermal conductivity k_{eff} was inversely proportional to A_i and followed the coherent potential model $(1 - 1.5f_v)$ for the three types of nanostructures considered. The coefficient of proportionality between k_{eff} and $(1 - 1.5f_v)/(A_i/4)$ was found to be $\beta = 5.38 \times 10^8 \text{ W/m}^2\cdot\text{K}$ and $\beta = 6.26 \times 10^8 \text{ W/m}^2\cdot\text{K}$ for nanoporous Si with cylindrical pores and vacancy defects, respectively. The difference in the value of β can be attributed to difference in temperature (500 or 300 K), interatomic potential (SW or Tersoff), pore or vacancy shapes, as well as spatial arrangement.

V. CONCLUSION

This study established that the effective thermal conductivity k_{eff} of crystalline nanoporous silicon predicted from non-equilibrium MD simulations was strongly affected by the pore interfacial area concentration A_i , the porosity f_v , and the system's length L_z . In addition, a modified effective medium approximation combining kinetic theory and the coherent potential approximation suggested that k_{eff} was proportional to $(1 - 1.5f_v)$ and inversely proportional to the sum $(A_i/4 + 1/L_z)$. This model agreed with MD simulation predictions for the thermal conductivity of crystalline nanoporous silicon with not only spherical pores (present study) but also with cylindrical pores and vacancy defects, reported in the literature.^{11,26} These results will be useful in designing nanostructured materials with desired thermal conductivity by tuning their morphology for various applications including thermoelectric energy conversion.

ACKNOWLEDGMENTS

The MD simulations were performed on the Hoffman2 cluster hosted by the Academic Technology Services (ATS) at University of California, Los Angeles.

¹A. G. Cullis, L. T. Canham, and P. D. J. Calcott, *J. Appl. Phys.* **82**, 909 (1997).

²G. Gesele, J. Linsmeier, J. Drach, J. Fricke, and R. Aren-Fischer, *J. Phys. D: Appl. Phys.* **30**, 2911 (1997).

³P. Roussel, V. Lysenko, B. Remaki, G. Delhomme, A. Dittmar, and D. Barbier, *Sens. Actuators A* **74**, 100 (1999).

⁴P. McCord, S.-L. Yau, and A. J. Bard, *Science* **257**, 68 (1992).

⁵D. Kovalev, V. Y. Timoshenko, N. Künzner, E. Gross, and F. Koch, *Phys. Rev. Lett.* **87**, 068301 (2001).

⁶F. V. Mikulec, J. D. Kirtland, and M. J. Sailor, *Adv. Mater.* **14**, 38 (2002).

⁷M. d. Plessis, *Sens. Actuators A* **135**, 666 (2007).

⁸M. d. Plessis, *Mater. Sci. Eng. B* **147**, 226 (2008).

⁹L. J. Currano and W. A. Churaman, *J. Microelectromech. Syst.* **18**, 799 (2009).

¹⁰C. R. Becker, S. Apperson, C. J. Morris, S. Gangopadhyay, L. J. Currano, W. A. Churaman, and C. R. Stoldt, *Nano Lett.* **11**, 803 (2011).

¹¹J.-H. Lee, J. C. Grossman, J. Reed, and G. A. Galli, *Appl. Phys. Lett.* **91**, 223110 (2007).

¹²J.-H. Lee, G. A. Galli, and J. C. Grossman, *Nano Lett.* **8**, 3750 (2008).

¹³A. Majumdar, *Science* **303**, 777 (2004).

¹⁴A. J. H. McGaughey, M. Kaviani, F. X. Alvarez, D. Jou, and A. Sellitto, *Adv. Heat Transfer* **39**, 169 (2006).

¹⁵M. P. Allen and D. J. Tildesley, *Computer Simulation of Liquids* (Oxford University Press, Oxford, UK, 2002).

¹⁶M. S. Green, *J. Chem. Phys.* **22**, 398 (1954).

¹⁷R. Kubo, M. Yokota, and S. Nakajima, *J. Phys. Soc. Jpn.* **12**, 1203 (1957).

¹⁸P. K. Schelling, S. R. Phillpot, and P. Keblinski, *Phys. Rev. B* **65**, 144306 (2002).

¹⁹F. Muller-Plathe, *J. Chem. Phys.* **106**, 6082 (1997).

²⁰D. A. McQuarrie, *Statistical Mechanics* (University Science Books, Sausalito, CA, 2000).

²¹J. Tersoff, *Phys. Rev. B* **39**, 5566 (1989).

²²Y. G. Yoon, R. Car, D. J. Srolovitz, and S. Scandolo, *Phys. Rev. B* **70**, 012302 (2004).

²³S. S. Mahajan, G. Subbarayan, and B. G. Sammakia, *Phys. Rev. E* **76**, 056701 (2007).

²⁴Z. Huang, Z. Tang, J. Yu, and S. Bai, *Physica B* **404**, 1790 (2009).

²⁵T. Coquil, J. Fang, and L. Pilon, *Int. J. Heat Mass Transfer* **54**, 4540 (2011).

²⁶Y. Lee, S. Lee, and G. S. Hwang, *Phys. Rev. B* **83**, 125202 (2011).

²⁷R. Prasher, *J. Appl. Phys.* **100**, 064302 (2006).

²⁸F. X. Alvarez, D. Jou, and A. Sellitto, *Appl. Phys. Lett.* **97**, 033103 (2010).

²⁹D. W. Song, W. N. Shen, B. Dunn, C. D. Moore, M. S. Goorsky, T. Radetic, R. Gronsky, and G. Chen, *Appl. Phys. Lett.* **84**, 1883 (2004).

³⁰H. Looyenga, *Physica* **31**, 401 (1965).

³¹J. Sturm, P. Grosse, and W. Theiß, *Zeitschrift für Physik B-Condensed Matter* **83**, 361 (1991).

³²R. A. Millikan, *Phys. Rev.* **22**, 1 (1923).

³³G. Chen, *Phys. Rev. B* **57**, 14958 (1998).

³⁴Y. S. Ju and K. E. Goodson, *Appl. Phys. Lett.* **74**, 3005 (1999).

³⁵M. G. Holland, *Phys. Rev.* **132**, 2461 (1963).

³⁶W. S. Capinski, H. J. Maris, E. Bauser, I. Silier, M. Asen-Palmer, T. Ruf, M. Cardona, and E. Gmelin, *Appl. Phys. Lett.* **71**, 2109 (1997).

³⁷S. J. Plimpton, *J. Comput. Phys.* **117**, 1 (1995).

³⁸S. G. Volz and G. Chen, *Phys. Rev. B* **61**, 2651 (2000).

³⁹Q. Tang, *Mol. Phys.* **102**, 1959 (2004).

⁴⁰F. H. Stillinger and T. A. Weber, *Phys. Rev. B* **31**, 5262 (1985).

⁴¹S. J. Cook and P. Clancy, *Phys. Rev. B* **47**, 7686 (1993).

⁴²M. D. Kluge, J. R. Ray, and A. Rahman, *J. Chem. Phys.* **85**, 4028 (1986).

⁴³J. Q. Broughton and X. P. Li, *Phys. Rev. B* **35**, 9120 (1987).

⁴⁴C. Oligschleger and J. C. Schön, *Phys. Rev. B* **59**, 4125 (1999).

⁴⁵D. P. Sellan, E. S. Landry, J. E. Turney, A. J. H. McGaughey, and C. H. Amon, *Phys. Rev. B* **81**, 214305 (2010).

⁴⁶N. Ramakrishnan, *Bull. Mater. Sci.* **17**, 499 (1994).

⁴⁷M. Marutake and T. Ikeda, *J. Phys. Soc. Jpn* **11**, 814 (1956).

⁴⁸W. A. Brantley, *J. Appl. Phys.* **44**, 534 (1973).

⁴⁹T. Coquil, E. K. Richman, N. Hutchinson, S. H. Tolbert, and L. Pilon, *J. Appl. Phys.* **106**, 034910 (2009).

⁵⁰B. Nait-Ali, K. Haberko, H. Vesteghem, J. Absi, and D. S. Smith, *J. Eur. Ceram. Soc.* **26**, 3567 (2006).

⁵¹H. W. Russell, *J. Am. Ceram. Soc.* **18**, 1 (1935).

⁵²A. Eucken, *Forschung auf dem Gebiet des Ingenieurwesens* **3**, 16 (1932).

⁵³P. E. Hopkins, P. T. Rakich, R. H. Olsson, I. F. El-kady, and L. M. Phinney, *Appl. Phys. Lett.* **95**, 161902 (2009).

⁵⁴D. Song and G. Chen, *Appl. Phys. Lett.* **84**, 687 (2004).

⁵⁵R. Landauer, *J. Appl. Phys.* **23**, 779 (1952).

⁵⁶D. G. Cahill and T. H. Allen, *Appl. Phys. Lett.* **65**, 309 (1994).

- ⁵⁷A. Minnich and G. Chen, *Appl. Phys. Lett.* **91**, 073105 (2007).
- ⁵⁸M.-S. Jeng, R. G. Yang, D. Song, and G. Chen, *ASME J. Heat Transfer* **130**, 042410 (2008).
- ⁵⁹K. M. Katika and L. Pilon, *J. Appl. Phys.* **103**, 114308 (2008).
- ⁶⁰T.-Y. Hsieh and J.-Y. Yang, *J. Appl. Phys.* **108**, 044306 (2010).
- ⁶¹J. M. Ziman, *Electrons and Phonons* (Oxford University Press, Oxford, UK, 1960).
- ⁶²J. W. Vandersande, *Phys. Rev. B* **15**, 2355 (1977).
- ⁶³P. Heino, *Eur. Phys. J. B* **60**, 171 (2007).
- ⁶⁴P. E. Hopkins, C. M. Reinke, M. F. Su, R. H. O. III, E. A. Shaner, Z. C. Leseman, J. R. Serrano, L. M. Phinney, and I. El-Kady, *Nano Lett.* **11**, 107 (2011).
- ⁶⁵M. S. Kushwaha, R. Helevi, G. Martinez, L. Dobrzynski, and B. Djafari-Rouhani, *Phys. Rev. B* **49**, 2313 (1994).